Marine Pollution Bulletin 127 (2018) 82–96

Contents lists available at ScienceDirect

Marine Pollution Bulletin

journal homepage: www.elsevier.com/locate/marpolbul

Baseline

Three-dimensional hydrodynamic modelling study of reverse estuarine circulation: Kuwait Bay

Y. Alosairi*, T. Pokavanich, N. Alsulaiman

Coastal Management Program, Environmental and Life Sciences Research Center, Kuwait Institute for Scientific Research, P.O. Box 24885, Safat, Kuwait

ARTICLE INFO

Keywords:
Inverse estuarine
Arid
Arabian Gulf
Baroclinic
Water exchange
Delft3D

ABSTRACT

Hydrodynamics and associated environmental processes have always been of major concern to coastal-dependent countries, such as Kuwait. This is due to the environmental impact that accompanies the economic and commercial activities along the coastal areas. In the current study, a three-dimensional numerical model is utilized to unveil the main dynamic and physical properties of Kuwait Bay during the critical season. The model performance over the summer months (June, July and August 2012) is assessed against comprehensive field measurements of water levels, velocity, temperature and salinity data before using the model to describe the circulation as driven by tides, gravitational convection and winds. The results showed that the baroclinic conditions in the Bay are mainly determined by the horizontal salinity gradient and to much less extent temperature gradient. The gradients stretched over the southern coast of the Bay where dense water is found at the inner and enclosed areas, while relatively lighter waters are found near the mouth of the Bay. This gradient imposed a reversed estuarine circulation at the main axis of the Bay, particularly during neap tides when landward flow near the surface and seaward flow near the bed are most evident. The results also revealed that the shallow areas, including Sulaibikhat and Jahra Bays, are well mixed and generally flow in the counter-clockwise direction. Clockwise circulations dominated the northern portion of the Bay, forming a sort of large eddy, while turbulent fields associated with tidal currents were localized near the headlands.

1. Introduction

Coastal dynamics have been utilized by man to disperse effluents so that, upon entering a marine system, they spread via various physical processes, such as turbulence and mixing, while biological activities play a role in rendering them harmless in the surrounding water (Alosairi et al., 2011). The temporal scale of the mixing and transport of effluents determines the effects of pollutants, for example, nutrients, on the biological activities in a marine system. On a spatial scale, the distributions of effluents are adjusted and gradually homogenized as one moves further away from the source in the receiving water. This is mainly attributed to the scale of the motion that a water body may experience, which is governed by the prevailing conditions. For example, estuaries that experience strong seasonal riverine discharges are subject to intense density-driven circulations compared to lower ones or during low seasons. Subsequently, this leads to enhanced hydrodynamics that may improve transport compared with well-mixed conditions, particularly in shallow waters. In addition, wind forces add an extra dimension to the complexity of water circulations, principally at the surface, which again contributes from a different perspective to transport and mixing. Henceforth, hydrodynamics of a water body should be well understood prior to any attempt to resolve the distributions of given water parameters.

Kuwait Bay, hereafter called 'the Bay,' is an elliptically shaped embayment that extends in the westward direction from the farthest north of the Arabian/Persian Gulf, hereafter called 'the Gulf,' as shown in Fig. 1. The Bay is characterized by comparatively shallow water throughout, and the depth ranges from 2 m near the coastal region to 18 m at the boundary with the Gulf estuary (Fig. 1). It covers an area of approximately 720 km^2 and has a boundary length of 20 km with the Gulf estuary. Due to the geographical location of the Bay, tides are mixed with predominantly semidurinal characteristics and experience some of the highest tidal range of the entire Gulf (occasionally > 4 m) (Alosairi et al., 2016). The coastal region of Kuwait is crucial as it serves most of the Kuwaiti population, particularly at the southern region of the Bay where $> 50\%$ of the population exists (Al-Rashidi et al., 2007). The coastal region is an important resource for the country, but it is a recipient of various suspended and dissolved materials, including nutrients, pollutants from oil transportation and sewage discharges (Alosairi et al., 2015). Furthermore, the Bay receives vast amounts of

* Corresponding author.
E-mail address: yosairi@kisr.edu.kw (Y. Alosairi).

https://doi.org/10.1016/j.marpolbul.2017.11.049
Received 3 July 2017; Received in revised form 13 November 2017; Accepted 22 November 2017

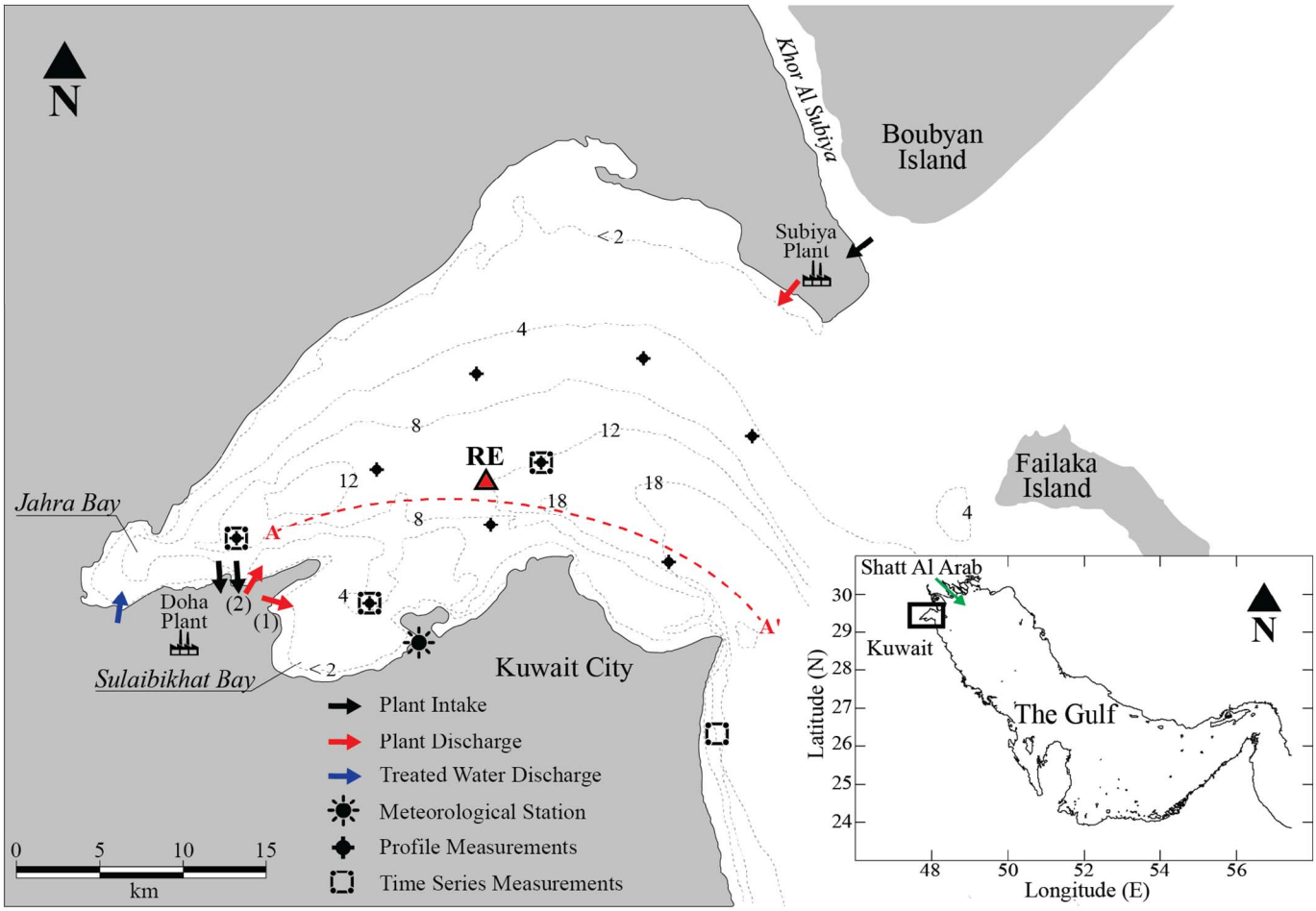

Fig. 1. Kuwait Bay physical characteristics and field measurement locations, RE is short of Reverse Estuarine and remarks the location where such assessment was conducted.

fine sediments originating from Shatt Al Arab and nearby areas, which is considered the main natural provider of fresh water to the northern Gulf region near the Bay (Alosairi and Pokavanich, 2017a, 2017b) (see Fig. 1). From a biological viewpoint, the Bay has intermittently experienced various algal blooms, particularly during warm seasons (Glibert et al., 2002), and has been categorized as a stressed water body within the Gulf. Thus, knowledge of hydrodynamics, including the circulations and flow fields, is fundamental for understanding the fate, transport and accumulation of solutes in the Bay. This would also enable the building of comprehensive management strategies and long-term monitoring plans for better water quality. Previously, limited studies were conducted to understand the hydrodynamics of the Bay. Pokavanich and Alosairi (2014) focused on the flushing characteristics but lacked detailed circulation assessments, while Rakha et al. (2010) studied the same topic but used a two-dimensional model. In the latter study, the model achieved reasonable fidelity with sea level observations and, to a lesser degree, with the tidal currents. However, the model is incapable of addressing material fluxes over time scales longer than the tidal cycle, e.g., spring-neap cycle, since the model omits the mean estuarine circulation by gravitational convection, and its renditions of the wind-driven flows are inherently improper.

The main aim of the present study is to investigate the spatial and temporal hydrodynamic characteristics of the Bay in a three-dimensional manner. The study is focused on the dynamics of the summer season when various environmental issues occur, specifically fishkill. This will be achieved by utilizing a numerical model in which the vital physical forcing parameters, including meteorological effects, will be considered in detail. Using the data of extensive field measurements conducted during the summer of 2012, the numerical model is validated. Following that, the model is used to study the Bay's prevailing hydrodynamics to reveal the residual circulations and the mean distributions of physical parameters. The work presented here is considered an important step towards understanding of the governing flow conditions in the Bay and other embayments within regions of similar arid hydro-environmental conditions.

The Gulf including the Bay is situated near the low northern latitudes and is close to the Tropic of Cancer (frequently referred to as the Northern Tropic), between longitudes of 48 and 59°E (Reynolds, 1993; Al-Sharhan et al., 2001). This area is recognized as one of the largest deserts in the World and is considered the boundary between tropical circulations and the synoptic weather systems of the mid to low latitudes (Reynolds, 1993; Al-Sharhan et al., 2001). Dry air between these latitudes generates clear skies and extremely arid conditions with limited precipitation and clouds (Al-Sharhan et al., 2001). In general, during the warm season, typically between May and October, the main path of the jet stream managing the passage of depressions passes north of the Pontic Mountains (Turkey) (Al-Sharhan et al., 2001). During the relatively cooler periods, typically November to February, the path of the jet stream shifts southwards and covers the northern region of the Gulf (Al-Sharhan et al., 2001). The Gulf climate, including the Bay, is characterized by high temperature, high relative humidity, limited precipitation and northwesterly winds (regionally known as 'Shamal' winds) that occur perennially (Al Senafi and Anis, 2015; Alosairi et al., 2011; Reynolds, 1993).

Similar to the previous hydrodynamic studies in the area (Alosairi and Pokavanich, 2017a, 2017b), the months June, July and August for the year 2012 are considered the main period representing the summer season for the current study. To further understand the prevailing

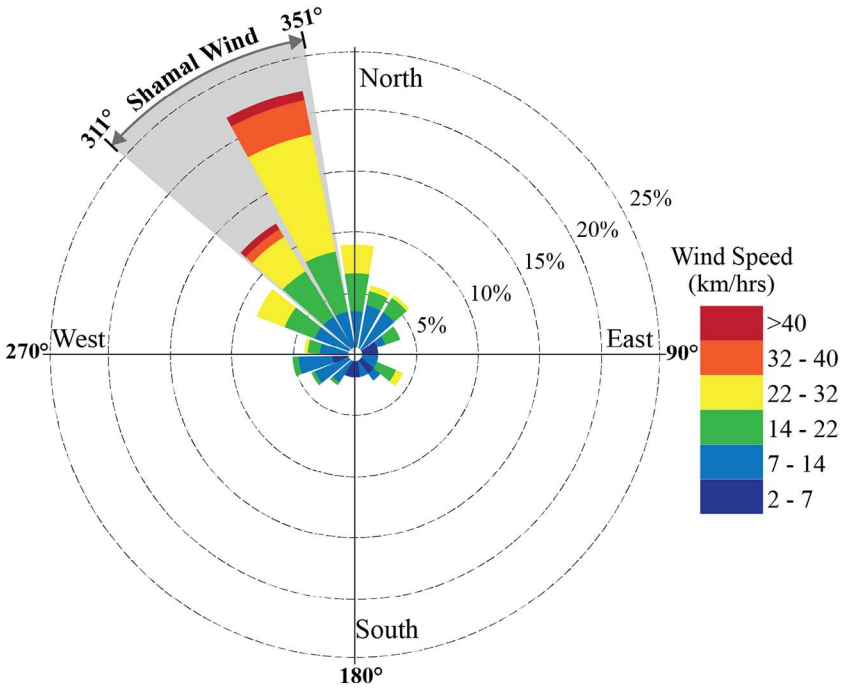

Fig. 2. Summer wind conditions of 2012, including the dominant wind direction 'Shamal.'

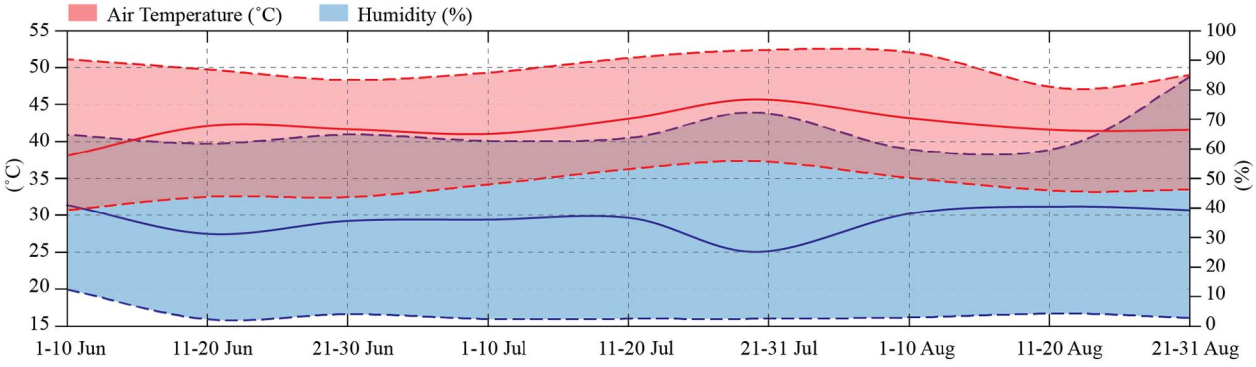

Fig. 3. Summer air temperature and relative humidity, the solid red line is the mean value of the air temperature, and the solid blue line is the mean value of the relative humidity, both averaged on 10 days basis. (For interpretation of the references to colour in this figure legend, the reader is referred to the web version of this article.)

summer conditions of the area, measured data were collected from a meteorological station neighbouring the study domain, as shown in Fig. 1. The measured parameters were collected on an hourly basis and included the wind direction, wind speed, solar radiation, air temperature and humidity. General statistical assessment confirms that the main wind during the summer season blows from the northwest direction of the Bay, in which the mean wind direction is calculated to be 331° from North, i.e., Shamal wind (Fig. 2). The maximum wind speed during this period rarely exceeds 11 m/s (≈ 40 km/h), as shown in Fig. 2, but it is virtually continuous; this is mainly linked to the relative strengths of the Arabian and Indian monsoonal lows and the associated steep pressure gradients (Al Senafi and Anis, 2015; Al-Sharhan et al., 2001; Reynolds, 1993). The average wind speed during this period is approximately 4.3 m/s (≈ 15 km/h). Similar to the trends of previous records (Al Senafi and Anis, 2015), the air temperature is extremely high, reaching 51 °C during July, and the mean value has been calculated to be 37 °C during summer (Fig. 3). The high air temperature, beyond 50 °C, is regionally known as 'Simoom' winds, and it is associated with the adiabatic rise and descent of the air passing the Zagros Mountains in north-west Iran from the east (Al Senafi and Anis, 2015). Although it has been reported in the same study that Simoom is common during May–June, in the current study, it is more evident during July (Fig. 3). Relative humidity readings fluctuate in a manner opposite of the air temperature readings, and this is mainly ascribed to the high air temperature that plays a role in reducing the relative humidity levels to below 30% during July (Fig. 3). The solar radiation during the summer period reaches 1010 W/m^2 during midday, but it sporadically decreases by 40%, i.e., 600 W/m^2, during this period owing to the occasional dust storm during summer. It is obvious to note that, during the summer season, precipitation and cloud cover are extremely rare.

From a hydrodynamic perspective, large and continuous discharges from either desalination plants or treated water will introduce various buoyant fields at several spatial levels. With horizontal density variation from the source of the discharge to offshore areas, an axial pressure gradient force will form that drives a non-tidal, gravitational convection mode of circulation (Weisberg and Zheng, 2006). Henceforth, special attention is given to the major discharges for accurate representation of the circulations in the Bay (Table 1).

Because of the limited water resources in the region, particularly Kuwait, desalination plants serve 90% of the population for freshwater needs, and two out of the three main plants of the country are located in the Bay, as shown in Fig. 1. Doha plant is located on the southern coast of the Bay, and it includes two intakes and two outflows, as illustrated in Fig. 1 and physically described in Table 1. The second plant, Subiya plant, is located on the northern headland of the Bay; the intake is

Table 1
Desalination plant locations and estimated discharges that were considered in the study.

Desalination plant	Discharge (m^3/s)	ΔS (ppt)	ΔT (°C)	Intake location		Outflow location	
				Long	Lat	Long	Lat
Subiya	110.0	5	3	48°9.922′E	29°33.225′N	48°9.907′E	29°33.236′N
Doha (1)	270.5	6	3	47°47.192′E	29°22.25′N	47°49.169′E	29°21.752′N
Doha (2)	50.5	6	3	47°47.770′E	29°22.231′N	47°48.233′E	29°22.238′N
Treated water		**Avg. S**	**Avg. T**				
Sulaibiya	1.6	1.7	28	–	–	47°43.732′E	29°21.389′N

located at Khor Al Sabiya, and the outflow is at the northern coast of the Bay. This has traditionally resulted in increased salinity levels, at least at the near fields, due to brine waste discharge associated with the desalination process (Hamoda, 2001). This effect is amplified due to the deteriorating trends of the freshwater discharge through Shatt Al-Arab (the only source of fresh water), which can balance the salinity levels in the Bay (Alosairi and Pokavanich, 2017a, 2017b). Along with those plants, thermal power plants are installed to generate electricity (Hamoda, 2001). Since the seawater is used for cooling purposes for the plants, it has a pronounced role in rising the water temperature locally and regionally in the Bay (Al-Banaa and Rakha, 2009; Al-Rashidi et al., 2007). It is worth noting at this stage that the intake/discharge, for the purpose of both desalination and power, uses the same outfall locations (Fig. 1 and Table 1). The estimated discharges of the plants and the general physical properties are given in Table 1.

Concerning the treated water discharges, one outfall is identified as the potential source of relatively large buoyant fields in the Bay. The outfall is located at the innermost regions of the Bay at Jahra (Fig. 1). The general physical characteristics of the discharge are associated with low salinity levels and intermediate-to-high temperatures (Table 1). Other storm water outfalls exist, particularly on the southern coast of the Bay. However, they are for the purpose of storm water and other unsystematic discharges that have very limited effects on the general hydrodynamics of the Bay, particularly during the dry season. Therefore, such discharges were neglected in the current study.

The main approach adopted to understand the prevailing dynamics of the Bay is field measurements of a spatial and temporal nature. Spatially, they cover the key dynamic features of the Bay, while temporally, they cover the typical neap-spring cycle (≈ 14 days). The measurements explained here were utilized to facilitate a detailed numerical modelling study of the entire summer season. In this regard, the following address the approaches in detail.

An intensive physical oceanographic measurement to understand the three-dimensional circulations of the Bay was carried out during the summer of 2012, spanning from 22 June to 16 July. Two types of measurements were conducted: time series and vertical profiles. The time series measurements include water levels, velocity profiles, temperature (near the surface and bed) and salinity (near the surface). With regards to the vertical profile measurements, widely distributed vertical transects were considered, as shown in Fig. 1. The profile measurements were conducted during two astronomical periods, spring and neap cycles, to highlight the dynamic significance of each period. These vertical profile measurements include temperature, salinity and density. Given that the tidal conditions are predominantly semidiurnal, it is worth noting that the profile measurements lasted for ≈ 6–6.5 h to cover all of the stations and minimize the mixing effects of the tides oscillations on the measured parameters. Further details regarding the measurements and the instruments used in the campaign are given in Table 2.

Three-dimensional, time- and density-dependent models are normally applied to coastal waters and estuaries to understand the circulations. The hydrodynamic numerical model named Delft3D-FLOW (Deltares, 2011) is applied in the present study. It is worth noting that Delft3D has successfully been applied to understand various dynamic aspects of the region in previous studies. Elshorbagy et al. (2006) applied the model to study the general dynamics of the Gulf, Elhakeem et al. (2015) studied long-term hydrodynamics of the same domain, and Alosairi and Pokavanich (2017a, 2017b) studied the seasonal circulations of the northern Gulf using the same model. At the Bay scale, the model was applied to study the flushing and residence time during the summer (Pokavanich and Alosairi, 2014). In addition, Alosairi and Pokavanich (2017a, 2017b) applied the model to assess the hydrodynamic impact associated with the reduction of Shatt Al Arab discharge on the northwest of the Gulf, including the Bay.

Delft3D simulates depth-averaged, i.e., two-dimensional (x and y), or layer-integrated, i.e., three-dimensional (x, y and z), unsteady flow and solute transport as a result of tidal forcing, meteorological effects or density-driven flows arising from temperature and/or salinity variations in the vertical and horizontal directions. In the vertical direction (z), the model is able to incorporate sigma (σ) coordinates with a non-uniform thickness layer, in which it is not firmly horizontal but instead smoothly follows the topography and the free surface. Most advantageous, the equations are formulated in orthogonal curvilinear coordinates or in spherical coordinates on the globe, which is important for large water bodies. This enables application of the model to various water bodies, including estuaries, lagoons, rivers, and lakes. Delft3D-FLOW solves the unsteady shallow water equations, including the horizontal equations of motion, the continuity equation and the scalar transport equations. For the current study area where the horizontal length scale (several km) is much larger than the vertical (several m), the shallow water assumptions are valid (Alosairi and Pokavanich 2017a). The model configurations for the current study solve the three-dimensional, hydrostatic, Boussinesq, Reynolds-averaged Navier-Stokes, and advection-diffusion equations to model the hydrodynamics, including temperature and salinity, by mainly utilizing the Alternating Direction Implicit (ADI) scheme (Deltares, 2011). Delft3D also considers the flooding and drying processes, which is vital for areas such as the Sulaibikhat and Jahra Bays (Fig. 1).

The following model configurations are used to validate Delft3D-FLOW during the summer season from 22 June to 16 July 2012. The modelling approach implemented involves a non-uniform curvilinear grid, generated using RGFGRID software, with a horizontal resolution that varies from 770 m at the open boundary of the modelling domain, namely, B1 and B2, while higher grid resolutions are adopted towards the inner parts of the Bay, with a typical size of 160 m which is almost 5 times smaller than those at the boundary (Fig. 4). This grid setup is vital to capture the horizontal buoyant fields interactions, particularly those that arise from the plant discharges in Sulaibikhat Bay (Pokavanich and Alosairi, 2014). In the vertical direction (z), sigma coordinates are used, and 10 layers with varying thickness were adopted. From the top, the first 3 layers are each assigned to be 5% of the total depth, then layers 4 through 7 are each 10%, and the remaining layers account for the final 15%. Such configurations were necessary to account for the effects of wind on the surface waters, as well as the baroclinic circulations resulting from the varying temperature and salinity during the season. The total number of initial surface wet grid cells is 20,482. To optimize the computational efficiency for the given grid resolutions, a time step of 30 s is necessary to ensure the Courant-Friedrichs-Lewy conditions. The bathymetric information and the coastline of the modelled domain

Table 2
Time series measurement details from 22 June to 16 July 2012 except for KB6 salinity measurements from 22 June to 7 July 2012.

	Station	Parameter	Instrument	Frequency	Depth (m)
Time series	KB1	Surface water level (WL) Velocity (V) Temperature (T): (*Near the surface and near the bed*) Salinity (S): (*Near the surface*)	Acoustic Doppler Current Profiler (ADCP) Sentinel 600 kHz ADCP (RD Instrument, USA) Infinity-Conductivity Temperature (CTW) (JFE Advantech Co. Japan)	5 min	12
	KB3	Surface water level (WL)	Autonomous measurement of the HOBO-WLL (Onset Inc., USA)	10 min	14
	KB5	Surface water level (WL) Velocity (V)	Acoustic Doppler Current Profiler (ADCP) Sentinel 600 kHz ADCP (RD Instrument, USA)	5 min	12
	KB6	Temperature (T) (*Near the surface and near the bed*) Salinity (S): (*Near the surface*)	Infinity-Conductivity Temperature (CTW) (JFE Advantech Co. Japan)	5 min	13
Profile	See Fig. 1	Temperature (T) Salinity (S) Density	In situ profile measurement AAQ-1183 (JFE Advantech Co, Japan)	During Neap (27-6-2012) and Spring (4-7-2012)	

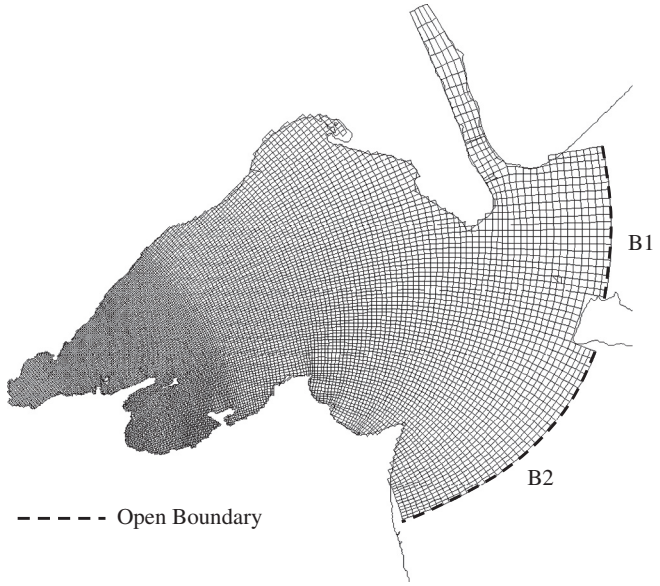

Fig. 4. The curvilinear numerical model grid utilized to discretize the modelling domain.

were obtained from EOMAP using Satellite Derived Bathymetry (SDB) techniques. A 5-m spatial resolution was obtained using Digital Surface Model (DSM) for the coastal areas of the Bay. For numerical modelling purposes, the bathymetric data was validated with field measurements to ensure its reliability. QUICKIN, companion software to the Delft3D suite, is used to interpolate the depth for each grid cell. For the heat flux model associated with metrology, the Murakami model was utilized. Briefly, the model considers the effective back radiation and heat losses due to evaporation and convection. In addition, the incoming radiation is absorbed as a function of depth in the model. The model is further explained from a modelling perspective in Deltares (2011) and theoretically in Murakami et al. (1985). For the three-dimensional turbulence, the k-Epsilon model was utilized, in which transport equations are solved for both the turbulent kinetic energy and energy dissipation (Deltares, 2011). Other numerical parameters utilized in the model are given in Table 3, which have values similar to those given in Pokavanich and Alosairi (2014) and Alosairi and Pokavanich (2017a, 2017b).

2. Model boundary forcing and initial conditions

Forcing and initializing an estuary model remains one of the key elements for precise validation with the field measurements and consequently leads to reliable model results. In general, there are two methods for providing the boundary forcing. The first is by using field measurements along (or near) the open boundary of the model, and the second is by nesting fine-to-coarse grid models so that boundary conditions can be obtained. The first method provides better representations of the model than those computed by the second method. However, in cases where boundary data is not available at the boundary or during the period of interest, it is practical to utilize a validated model, i.e., the second approach. In the current study, boundary forcing data were mainly obtained from the well-validated model of the Northern Arabian Gulf (NAG) explained in Alosairi and Pokavanich (2017a, 2017b).

To understand the characteristics of the water levels at the model boundaries B1 and B2, the water level computations of the summer season (90 days) were extracted from the NAG model. The two prominent spikes shown in periodogram of Fig. 5 are indicative of the mixed nature of the tides at the boundaries. The strong semi-diurnal and diurnal signals are attributed to the tidal constituents M_2 and K_1, as they fall at their signature frequencies of 1.932 and 1.002 (cycles per day) respectively.

This is confirmed by the results of the least squares tidal harmonic analysis performed on the 90-day record using WORLD TIDE, a MATLAB application for the analysis and prediction of tides (Boon, 2006). As expected, M_2 was the main contributor to total variation of water levels, followed by K_1, O_1, S_2, and lastly N_2. The relative strength between the amplitudes of the diurnal to the semi-diurnal constituents gives the tides a form number of 0.841. Tides with a form number between 0.25 and 1.5 are categorized under the mixed, predominantly semi-diurnal category (Boon, 2013). It should be noted that the harmonic analysis was performed only for the five principle tidal constituents listed in Table 4. Astronomical tides generated by the constituents have accounted for 95.06% of the total variation in the simulated boundary water levels, with an RMS error of 0.171 m, hence, they give a reasonable description for the characteristics of the water levels at the model boundaries. As for the 5% residual water levels, they

Table 3
Numerical parameters utilized in the model.

Water density (kg/m^3)	Wind drag (at 25 m/s)	Horizontal viscosity (m^2/s)	Horizontal diffusivity (m^2/s)	Secchi depth (m)	Dalton number (dimensionless)	Manning coefficient (dimensionless)
1028	0.0027	5	10	4	0.0006	0.026

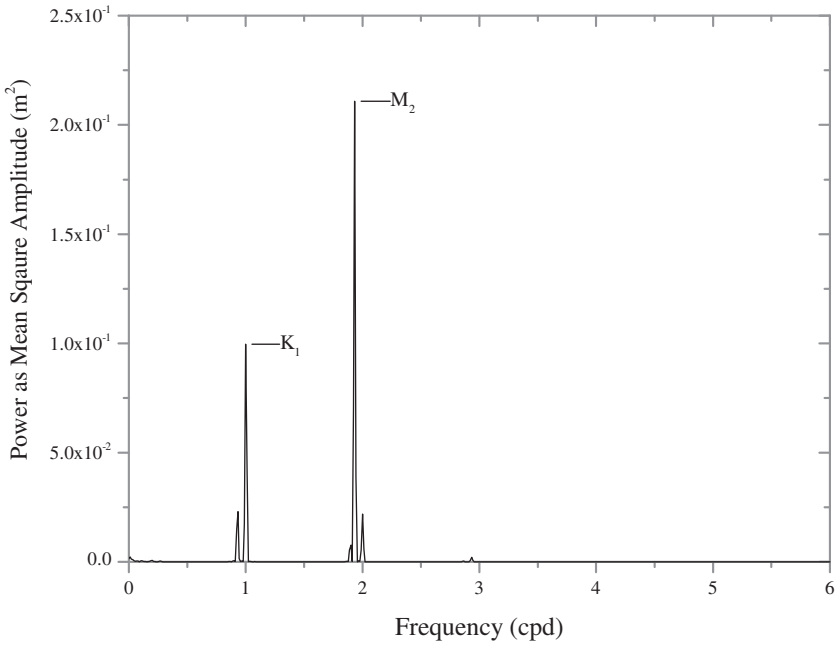

Fig. 5. Power spectral density (PSD) of the water levels at the model boundaries using Fast Fourier Transform (FFT) and a Hanning window.

Table 4
Results of the tidal harmonic analysis at the model boundaries.

Tidal constituent	O_1	K_1	N_2	M_2	S2
Amplitude (m)	0.323	0.553	0.164	0.788	0.254
Phase (degree)	209.62	306.08	155.69	279.42	44.31
Tidal constituent frequency (cpd)	0.929	1.002	1.895	1.932	2.000
Tidal form number $F = \frac{K_1+O_1}{M_2+S_2}$	0.841				

are likely attributed to two sources: additional astronomical tidal constituents which were not included in the harmonic analysis due to the limitations imposed by the length of the analyzed water level record, and non-tidal meteorological forcing that cannot be captured by tidal analysis.

The boundaries, B1 and B2, were forced with temperature and salinity data on an hourly basis and throughout the model layers using the NAG model. Due to space limitations, individual data of the open boundaries cannot be presented here; alternatively, the monthly averaged values of temperature and salinity during the summer are summarized in Table 5. The mean temperature values at B1 and B2 do not differ significantly, except that B1 is slightly elevated by at least 1 °C. This is due to the bathymetric nature at the boundaries. The salinity forcing at the boundaries differs in an opposite manner compared to the temperature. At B1, the salinity levels are lower than those at B2 by approximately 2 ppt. This replicates the effects of the nearby Shatt Al Arab discharge, which is the main source of freshwater to the region (Fig. 1). With regards to meteorological forcing, parameters including wind speed and direction, air temperature, relative humidity and air pressure were introduced in a uniform manner over the model domain. These effects were applied at 10 m above mean sea level on an hourly basis as per the values given in Figs. 2 and 3. For the discharges of the desalination plants and treated water, they were applied on a continuous basis throughout the simulation period, as per Table 1. Such discharge assumptions are adequate since they only cease/reduce during the maintenance period that lasts for a few hours according to the Ministry of Electricity and Water and the Ministry of Public Works (Kuwait) operations.

Table 5
Monthly mean value model boundary forcing of temperature and salinity during summer.

Boundary	Temperature (°C)			Salinity (ppt)		
	June	July	August	June	July	August
B1	29.7	32.3	32.1	39.9	40.5	39.7
B2	28.8	31.5	32.2	42.6	43.3	43.3

The initial values of water elevation and velocity are set to stagnant (zero) all through the computational domain. The initial values of the temperature and the salinity were set to 27.3 °C and 44.2 ppt, respectively, throughout the domain. However, to achieve representative initial baroclinc conditions, a spin-up time of several days was allowed. This is following the flushing time of the Bay, which is estimated to be 45 days in Pokavanich and Alosairi (2014). It is worth noting that, during the spin-up period of the model, meteorological and discharge effects were included.

To ensure adequate performance of the model, the computed results are directly compared with the field measurements during the summer season of 2012. With the abundance of field measurements, as shown in Fig. 1 and detailed in Table 1, this has enabled sufficient evaluation of the model results in a three-dimensional manner. Three types of comparisons are performed: time-series, scatter plot (for velocity), and spatial distributions of physical parameters at the sea surface and near the bed.

Time-series comparisons between the observed and modelled sea levels at KB1, KB3 and KB5 are shown in Fig. 6, and the wind velocity vectors that were uniformly used to force the model are presented in the same figure. An accurate agreement in both phase and amplitude has been achieved for the three locations. Although the tides followed a similar rhythm in all stations, gradually increasing tidal ranges are observed from KB1 (outside the Bay) moving towards KB5 (inside the Bay). At KB1, KB3 and KB5, the maximum water level ranges during the model validation period were 3.6, 4.4 and 4.6 m, respectively. Having said that, the model adequately managed to follow such variations in the three assessed locations. The model also reproduced the neap-spring cycle at all of the stations. This also confirms the validity of using the tidal constituents, addressed previously in Table 4 and Fig. 5, to represent the water levels characteristics in the Bay.

The model computations of the velocity were compared with field measurements at two levels, near the surface and near the bed, for two stations, KB5 and KB1 (Fig. 7). Unlike the water levels, the velocity variations are relatively higher in both magnitude and direction from

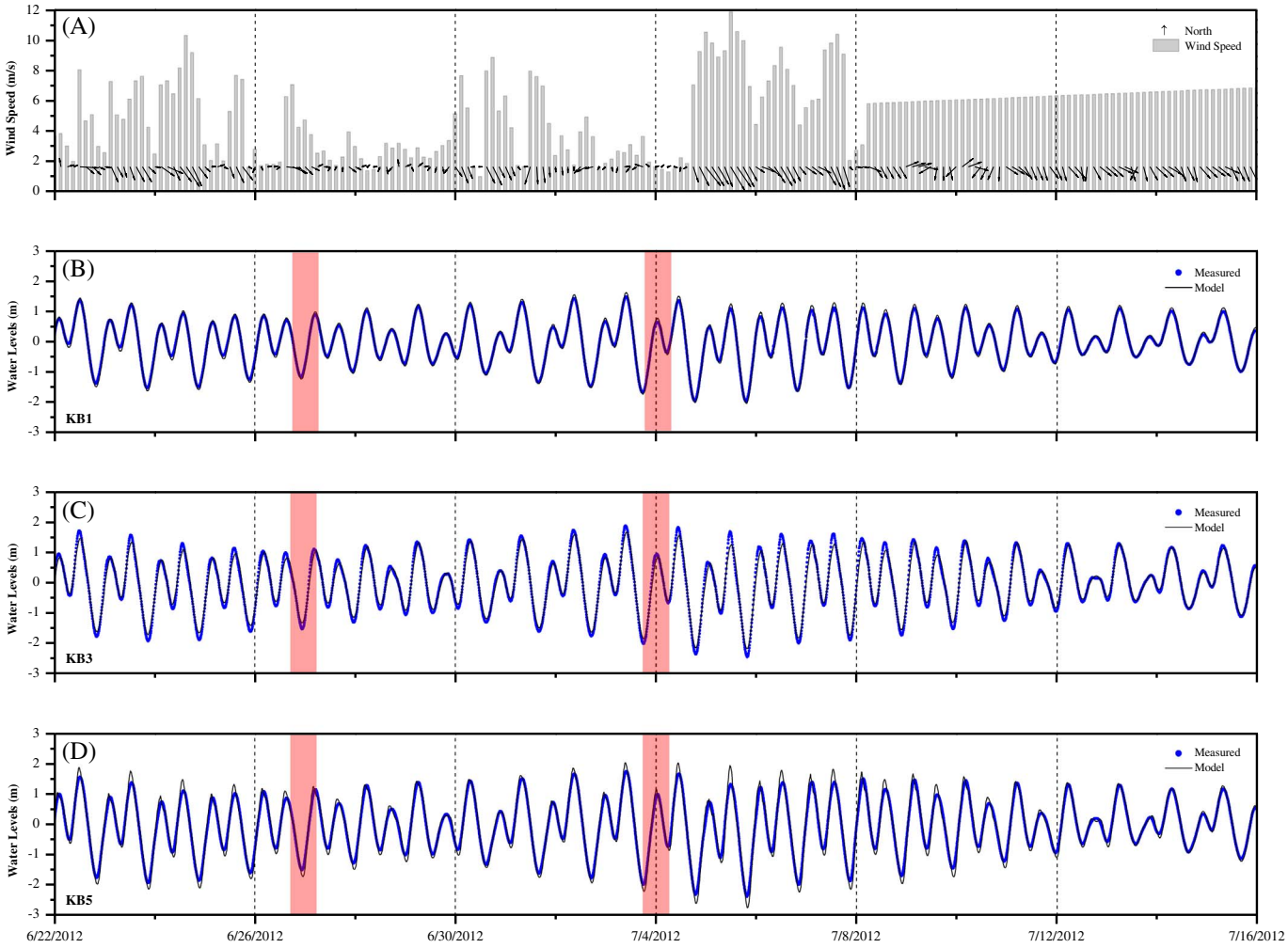

Fig. 6. Comparisons between the measured and computed water levels and the corresponding wind conditions in A. The shaded red lines denote the synoptic surveys for station KB1 (B), KB3 (C), and KB5 (D); the first is during the neap cycle, and the second is during the spring cycle. (For interpretation of the references to colour in this figure legend, the reader is referred to the web version of this article.)

one location to another, reflecting the irregular coastline and bathymetric characteristics. Such physical variation may lead to intrinsic differences between the model computations and the field data. In general, the model performed reasonably well when compared to the field measurements in KB1, but lower accuracy is computed in KB5. Such a discrepancy is likely associated with the layer representations of the model and vertical adaptation of the layer-integrated assumption. At station KB5, the current is lower than at KB1 (rarely exceeding 0.3 m/s for the former and reaching almost 1.0 m/s for the latter). Noticeably, there is a difference in the current velocity between near to the bed and the surface layers at both stations. In KB1, the velocity at the surface is higher by 12% than near to the bed; however, in KB5, the difference is only 3%. Although both stations are in similar depth ranges of approximately 12 m, the variations in velocity are mainly attributed to the typographical nature of the region. That said, the overall current computations are assumed to be acceptable for the purpose of the study.

Having seen the reasonable temporal performance of the model at KB1 and KB5, Fig. 8 presents the spatial depth averaged flow fields of the modelled domain during spring and neap tides. The magnitude of the flow fields correlated well with the tide conditions. Weaker flow fields are computed during the neap tides (≈ 2.3-m tidal range) compared to the spring tides (> 4.3-m tidal range). In particular, strong currents are represented by the model at the mouth of Sulaibikhat Bay due to the large volume of water that is contracted during the flood conditions of the spring tide (Fig. 8B). Other headlands on the southern coast of the Bay are also responsible for creating a strong flow regime associated with eddies over the tidal cycle, specifically during spring tides (Fig. 8B). In contrast, during neap tides, the currents smoothly followed the coastline and the deeper channel of the Bay (Fig. 8A). In general, weak flow fields are computed at the shallow regions, including Jahra Bay, Sulaibikhat Bay and the northern coast of the Bay, which has ordinary flow features.

The temperature computations were validated using comprehensive sets of time series measurements at KB1 and KB6, as well as synoptic profile measurements to account for both horizontal and vertical temperature distributions. For the time series measurements, two levels were considered, near the bed and near the surface (Fig. 9). In general, the model results are in fair agreement with the measured data, particularly at KB1. Although the temperatures at KB1 did not vary significantly near the bed (29.8–31.2 °C), periodic increases associated with metrological effects are well computed at the surface with minimal discrepancies (Fig. 9A). High peaks and well-defined patterns are observed in KB6 throughout the depth. Such stronger peaks are associated with the shallow nature of the area and the combined effects of the nearby Doha plant discharges and meteorology. This has resulted in daily variations at KB6 of ≈ 2.5 °C fluctuating between the cyclic motion of the water (Fig. 9B and D). The model computations at KB6 were in phase with the measured data but over-predict the temperature levels by 1 °C. Perhaps such a discrepancy is associated with the bathymetric

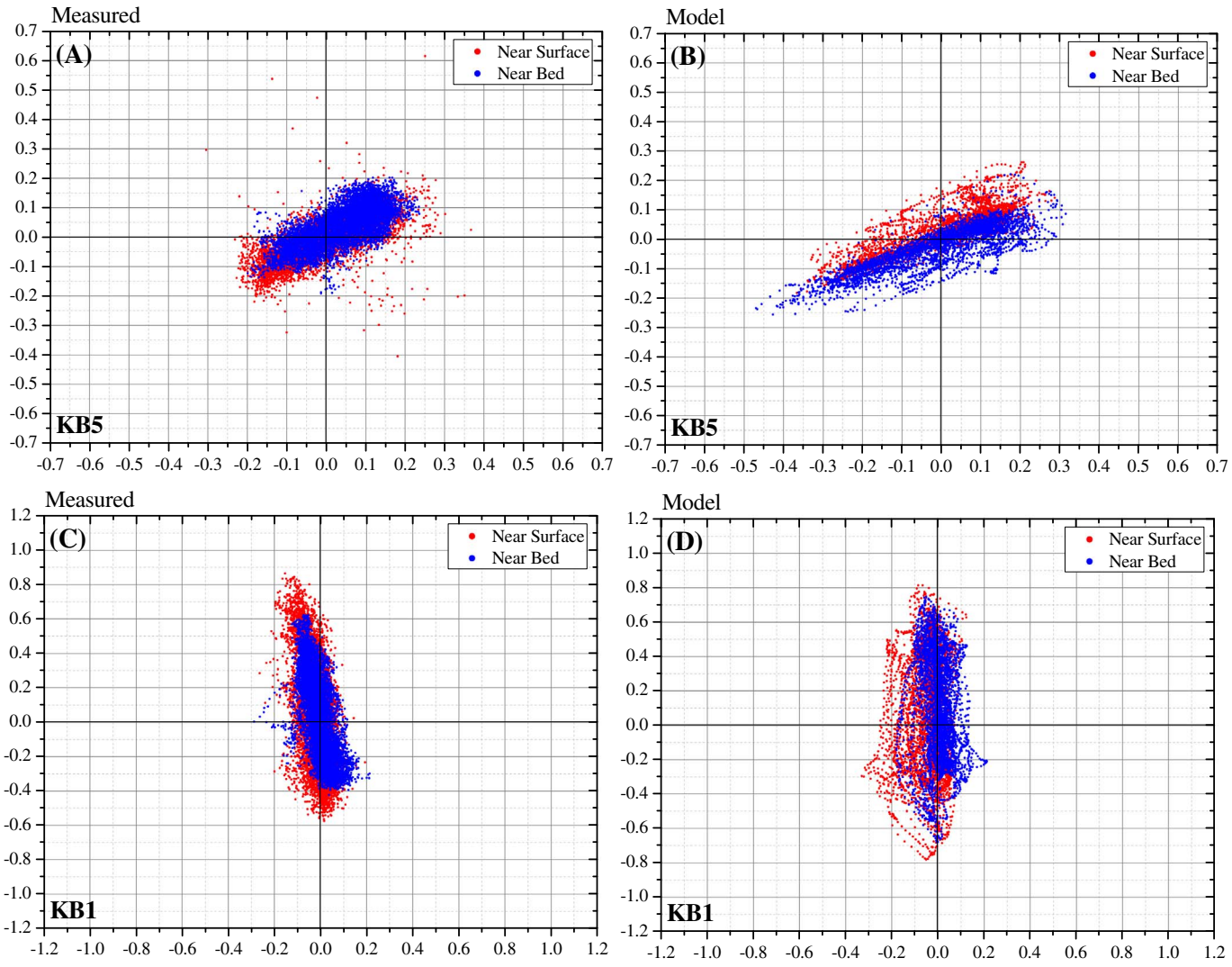

Fig. 7. Comparisons between the measured and computed velocities near the surface and bed at stations KB1 and KB5; panels A and C present the measured velocities, and panels B and D present the computed velocities.

or horizontal grid representations. However, the model was able to replicate the strong variability between the two locations and at two vertical levels.

In addition to time series comparisons between the model results and measurements, the spatial distributions of the temperature near the surface and the bed were compared using the profile measurements as per the locations shown in Fig. 1. To ensure the performance of the model during the neap-spring cycle, two conditions were considered: the 27 June 2012 survey for the neap cycle and the 4 July 2012 survey for the spring cycle. For sensible and direct comparison purposes, the profile measurements were averaged to account for 5% and 15% of the total depth at each location and for both levels near the surface and near the bed, respectively. This is to match the layer-integrated assumption of the model, for which 5% and 15% of the total depth represent the surface and bed layers, respectively. Finally, the data were horizontally interpolated for each layer and directly compared as shown in Figs. 10 and 11 during the neap and spring cycles, respectively.

It is important to mention that, with the detailed model setups, disagreements between the 'instantaneous' model results and the 'horizontally interpolated' field measurements are expected in this exercise for two fundamental reasons: first, due to the time lag between the profiles since they were conducted sequentially and typically took 6–6.5 h to complete for each survey; and second, high frequency climatic events such as wind regime or tide shifts during the measurement period could introduce a slight alteration, particularly at the surface layer or in the shallow waters. Such explanations apply to all parameters considered for the same spatial comparisons, including salinity and density.

Visually, the model results compared well with the measured profiles during both cycles, neap and spring, and at both levels, near the surface and the bed (Figs. 10 and 11). During the neap cycle, there is a clear temperature variation between the surface and bed layers of $\approx 1.3\ ^{\circ}C$. To a similar extent, the variations were achieved during the spring cycle, but with higher temperatures associated with the meteorological effects of July. The model performed very well in computing such variations during both cycles with minor discrepancies.

In a similar manner to temperature, the salinity levels were validated. Due to data availability, the time series measurements of the salinity were only compared with the model near the surface for the two stations KB1 and KB6. The salinity levels at the KB1 station had trivial variations throughout the validation period, with a mean value of 43 ppt. At KB6, a prominent semi-diurnal signal, with a periodic 3 ppt pulses added to the background concentration is shown in Fig. 12B. This is attributed to the interaction of the Doha plant plume with existing tidal condition. It is worth noting that the mean difference between KB1 (outside the Bay) and KB6 (inside the Bay) is approximately 3.5 ppt. That being said, accurate model computations were

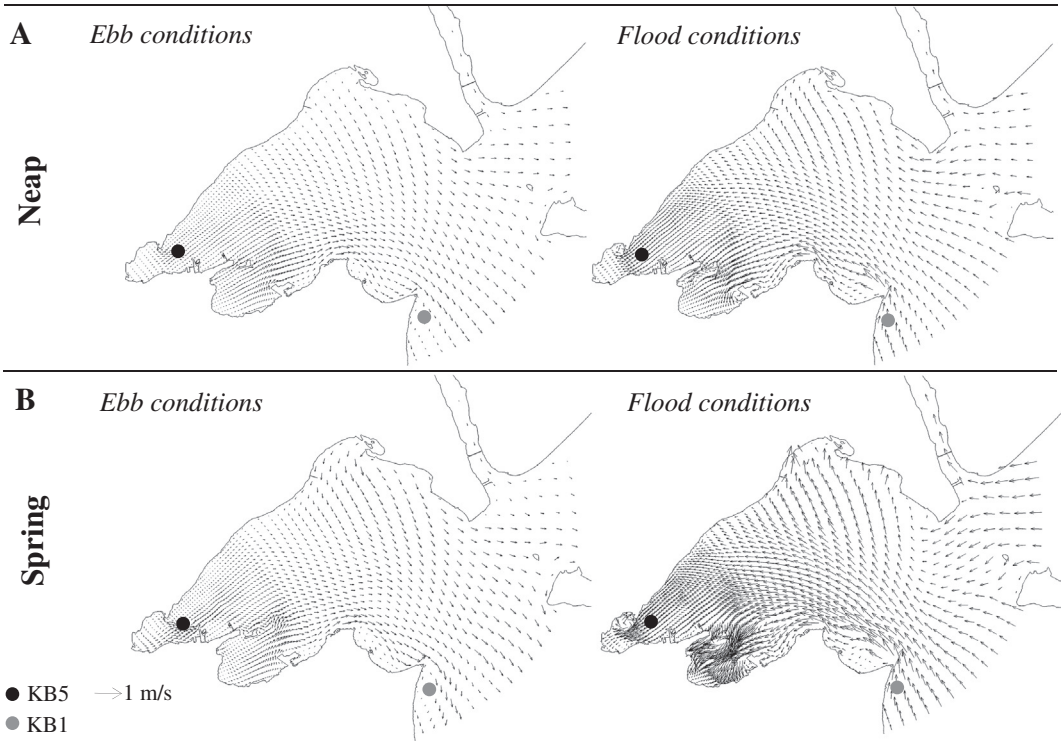

Fig. 8. Snapshot of the computed depth-averaged velocities during ebb and flood conditions in A: the neap cycle B: the spring cycle.

achieved in both stations, reflecting the adequate boundary forcing, including the point source discharges and meteorological representations. The mixing and transport salt model were able to reproduce the local variations, as in KB6, and the offshore region, as in KB1, which indeed adds to the reliability of the model results. For the detailed spatial distributions (Figs. 10 and 11), the model was also able to reproduce the horizontal variations in the Bay throughout the water column. Despite the data limitations of the time series, the model simulated the salinity transport processes satisfactorily over the neap-spring cycle, at both the surface and near the bed (Figs. 10 and 11).

The performance assessment of the model was concluded by comparing the spatial distributions of the model results and the

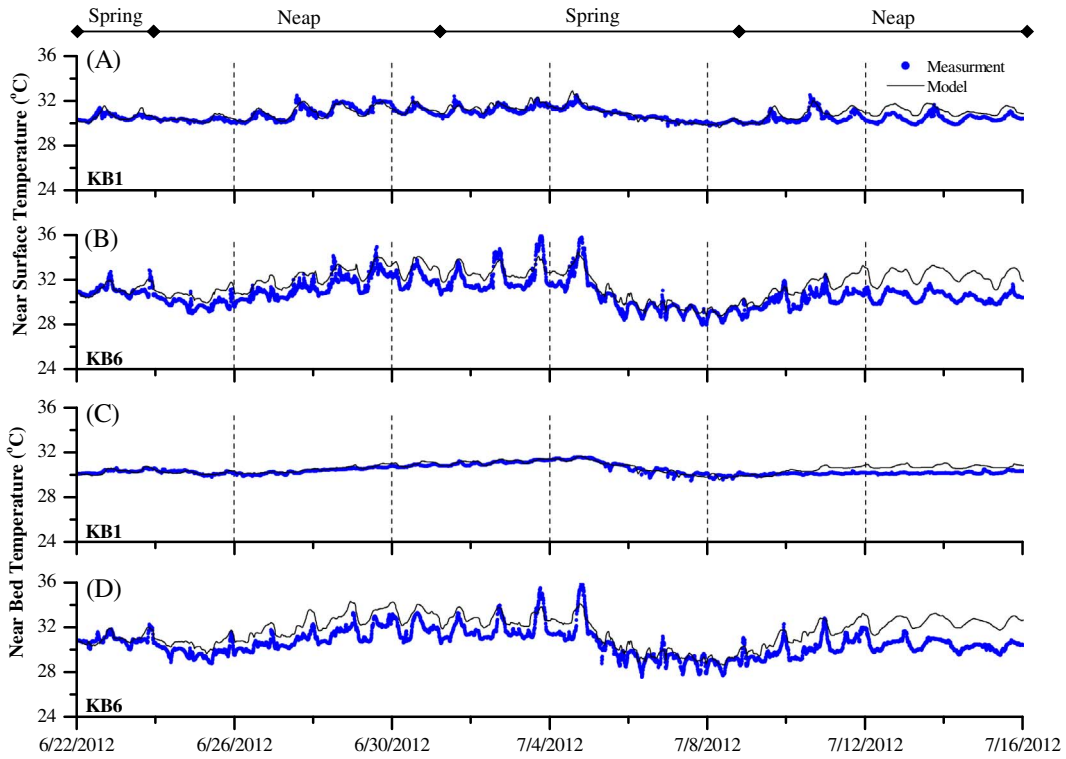

Fig. 9. Comparisons between the measured and computed time series of temperature: panels A and B for near the surface and panels C and D for near the bed at stations KB1 and KB6.

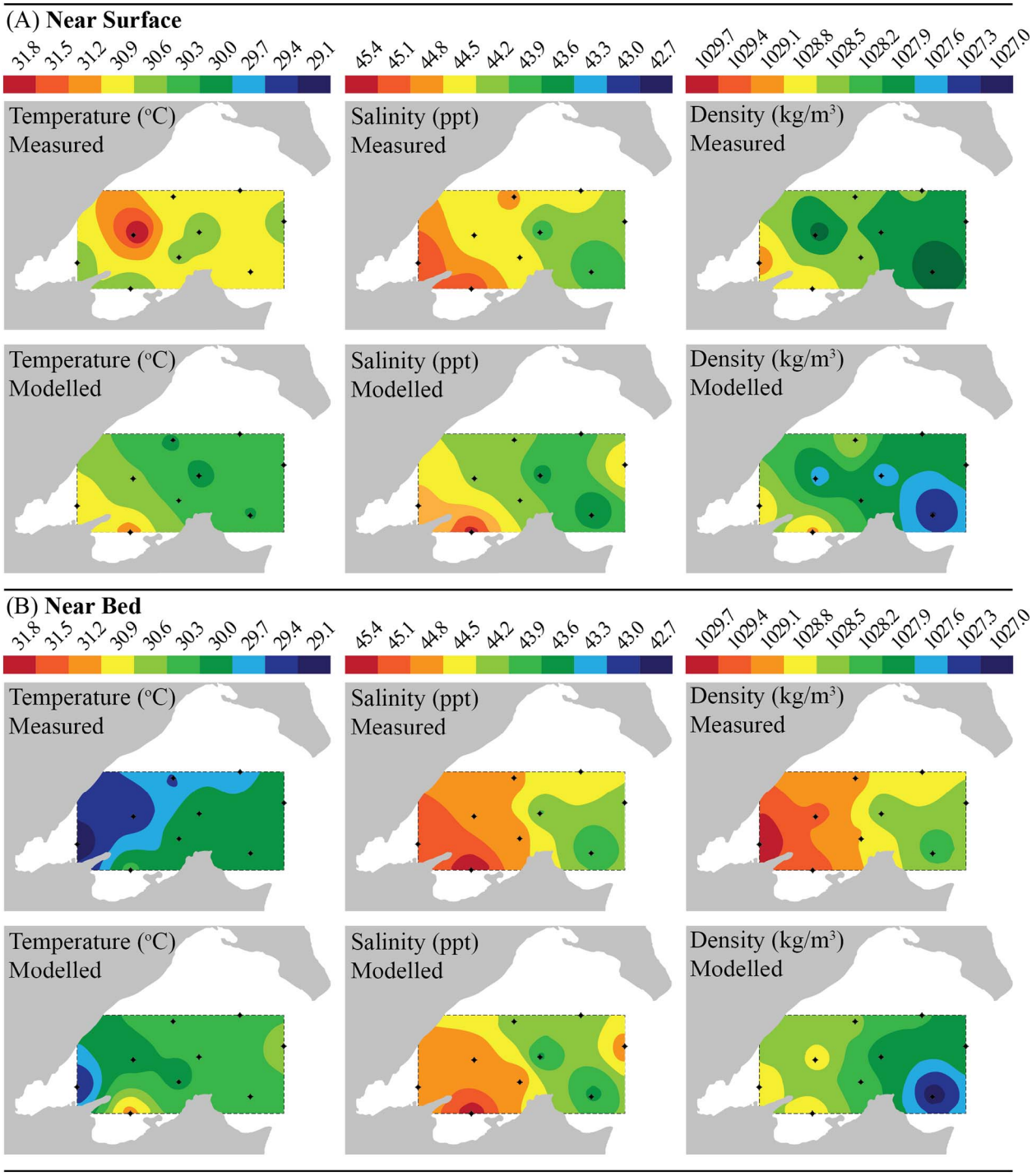

Fig. 10. Comparisons between the measured and computed spatial distributions of temperature, salinity and density during the neap cycle: A near the surface, B near the bed.

measurements in a similar manner to the temperature and salinity (Figs. 10 and 11). It is evident that, during the assessed cycles, dense waters resided in the lower portions of the water column in the Bay with horizontal gradients. Visually speaking, the horizontal variations followed similar trends to the salinity levels extending from Jahra Bay towards the mouth, with the prior being higher than the latter by at least 2 kg/m^3. Again, with reasonable discrepancies, the model followed similar patterns to the measured data (Figs. 10 and 11).

Since the key physical parameters were simulated and validated reasonably against the field measurements using the Delft3D-FLOW model, they were utilized to assess the horizontal and vertical summer mean levels of temperature, salinity, and density and the residual circulations for the modelled domain. This is achieved by performing Fourier Analyses over the summer season (Deltares, 2011). The distributions of temperature, salinity and density are first explained, followed by a discussion on residual circulations.

The horizontal mean distributions during the summer season are given in Fig. 13 for temperature, salinity, and density, while for the vertical distributions along the A-A′ section, the main axis of the Bay (see Fig. 1) is given in Fig. 14. It is important to mention that the modelled distributions of the parameters presented here are a result of the interplay among the buoyant fluxes, advection by tides and winds, and mixing processes during the summer season. In general, the distributions indicate that the warm-saline waters mainly occupy the

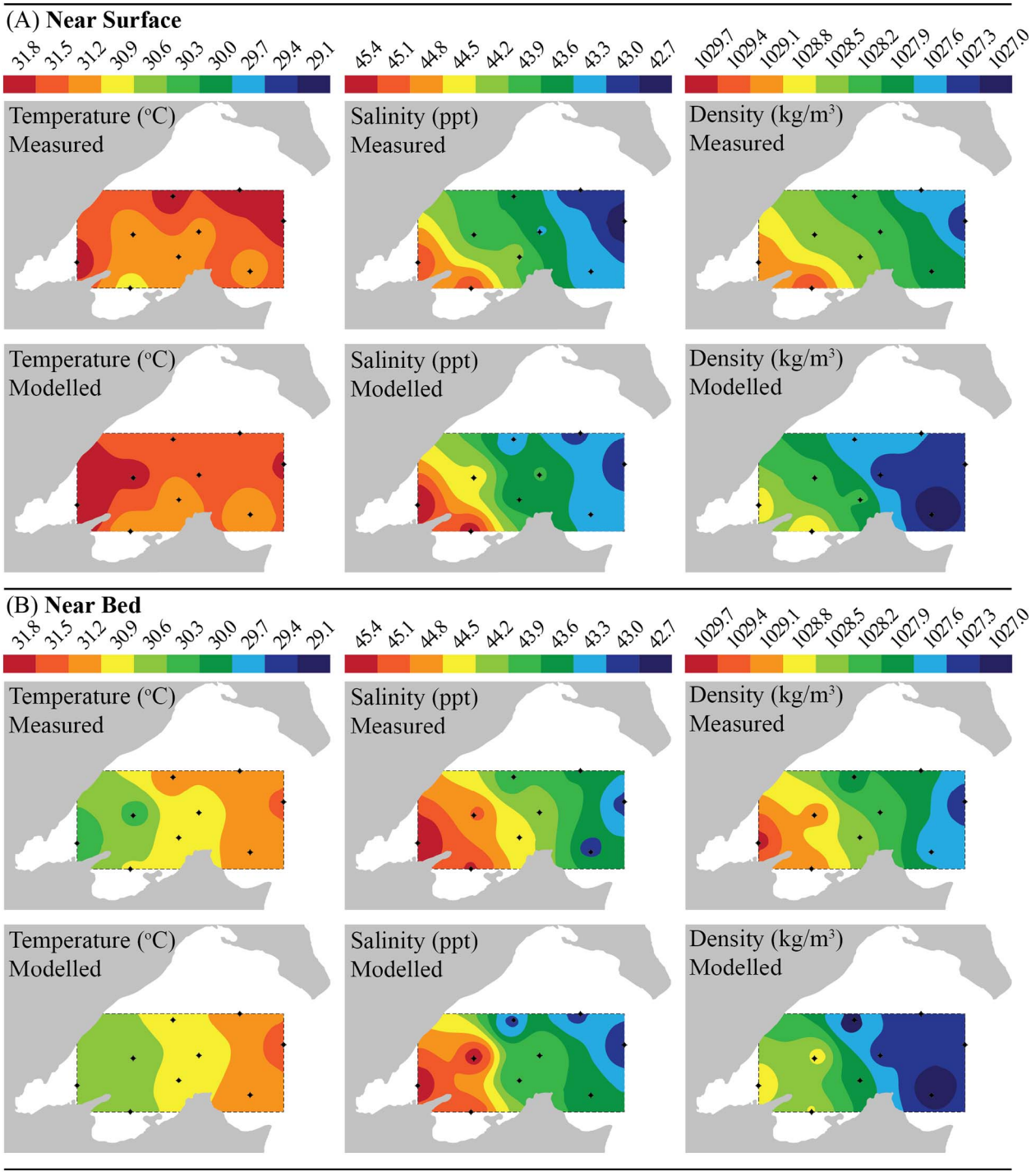

Fig. 11. Comparisons between the measured and computed spatial distributions of temperature, salinity and density during the spring cycle: A near the surface, B near the bed.

innermost portions of the Bay (Fig. 13A and B). As a result, this imposed clear density gradients, horizontally and, to a lesser extent, vertically (Figs. 13C and 14C). The highest temperatures in the Bay are found in the shallow regions, specifically at Sulaibikhat Bay, where the mean values reached 35 °C (Fig. 13A). This is mainly associated with Doha desalination plant outflow, while those effects were very limited in Subiya due to the open nature of the region and the corresponding mixing processes. Horizontally, in the southeast to northwest direction, a large tongue of cool water (31 °C) is sandwiched between the warm-shallow waters, imposing another sort of horizontal temperature gradient but to a lesser extent (Fig. 13A). In the vertical direction along the A-A′ section, the shallow waters are almost mixed throughout the depth; however, in the deep waters (25 m), the formation of the thermocline is evident, and the temperature difference is almost 1 °C between the surface and the bed. The horizontal salinity distributions showed a gradual increase from 42 ppt at the offshore regions to 45 at the shallow areas (Fig. 13B). Again, Sulaibikhat and Jahra Bays are mainly characterized with the highest salinity levels, which are associated with the Doha desalination plant and mass loss due to excessive heat and evaporation. The two main headlands of Kuwait City compose the transition zone between the saline water of the shallow regions and the relative fresh waters of the offshore deeper areas. Distinctive to this region, the horizontal dispersion mechanisms associated with tidal currents (see Fig. 8) play a key role in weakening the thermohaline

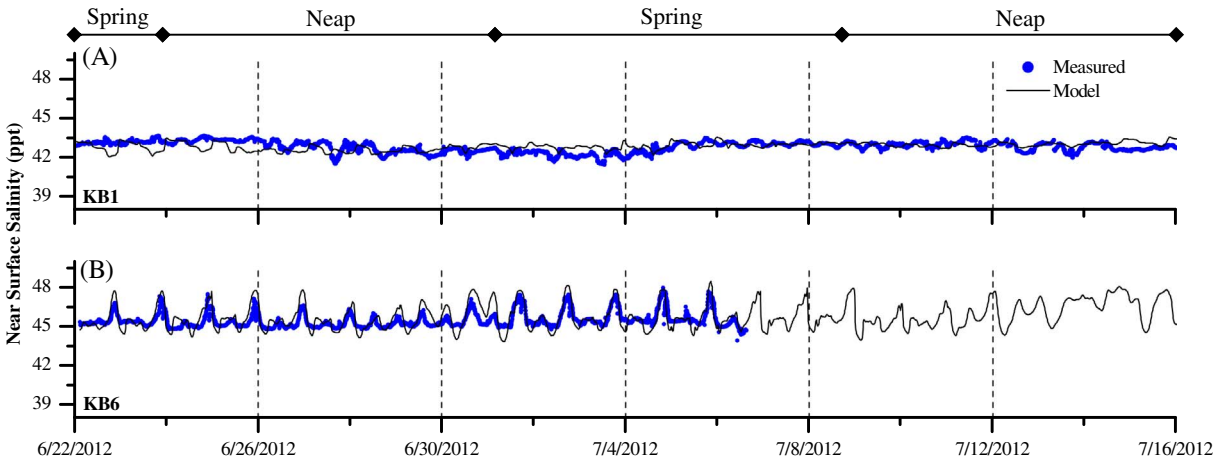

Fig. 12. Comparisons between the measured and computed time series of salinity: panels A and B for near to the surface and panels C and D for near to the bed at stations KB1 and KB6.

structure.

Along the A-A′ section, the longitudinal shear stress imposed by the bed friction and the tidal activities creates diagonally oriented gradients (Fig. 14). It is worth noting that the salinity gradients are more intense than the temperature gradients along the main axis of the Bay (Fig. 14A and B). The three-dimensional density structure followed similar forms of salinity where the water is densest (1030 kg/m^3) at the semi-enclosed Sulaibikhat Bay (Fig. 13C). This area is considered a great source of dense water to the remainder of the southern coast. Holistically, these conditions promote baroclinic (or gravitational) estuarine circulations that will be further explained later.

The water quality, as well as the corresponding estuarine ecosystem health, is strongly linked to its residual circulations. At short time scales, i.e., ≈ 6–12 h, tidal current fluctuations may introduce large fluxes of effluents, including nutrients. However, it is the net transport that governs the overall exchange of water matters along the axis of a typical estuary (Stacey et al., 2001). As a result, the understanding of residual circulation of the Bay is vital from both environmental and management perspectives. As shown in Fig. 14, the density gradient associated with the salinity would derive estuarine circulations, as fundamentally explained in Pritchard (1967). It is worth noting that, in classical estuarine conditions, the flow is seaward at the surface and landward near the bed. Such flow conditions are very dependent on the buoyant fields and are enhanced by the winds and bed settings. However, opposite configurations are found at the main axis of the Bay, and the flow is landward at the surface and seaward near the bed, leading to what is frequently called inverse (or reverse) estuarine circulation (Fig. 15). As the fresh waters progress from the surface landwards, the dense waters near the bed, which mainly originated from Sulaibikhat and Jahra Bays, flow seawards, as shown in Fig. 15. A longitudinal shear field is created at the main channel, section A-A′, where the light-surface currents are larger than the dense-bed currents, as depicted in Fig. 15. Arid climate, limited freshwater and runoff, and brine waste discharge from the desalination plant have shaped the reverse estuarine circulations in the Bay. It is not surprising that the Bay exhibits those conditions since similar circulations are found in arid climates elsewhere (Kämpf and Ellis, 2014). However, the extent of those conditions has been altered, particularly in the landward direction, due to the reductions in river flow patterns of Shatt Al Arab (Fig. 1) (Alosairi and Pokavanich, 2017a, 2017b). Those flow circumstances would result in several implications to the transport and concentration levels of various water quality parameters, but quantifying this is beyond the scope of the current study. Other turbulent features are existent in the Bay, particularly near the headlands that create eddies of several scales (Fig. 15). In Sulaibikhat Bay, the flow appears to be complex near the entrance, primarily due to the strong jet created by the Doha plant interacting with the strong tidal currents. The dominant flow directions in Sulaibikhat and Jahra are mainly counter-clockwise. At a larger scale, the northern half of the Bay is dominated by a large eddy acting in the clockwise direction (Fig. 15).

To examine the temporal variability of the flows that created the reverse estuarine circulations in the Bay, station RE, shown in Fig. 1, was considered to demonstrate the strength of the reverse estuarine circulations at the main axis of the Bay. The time frame for this assessment spanned from 15/6/2012 to 20/7/2012, which covered at least two spring-neap cycle and overlapped with the model validation period. An ideal low-pass filter with a cutoff frequency of 0.5 cpd was applied to the modelled east-west velocity profiles to capture the residual flow (Fig. 16).

In general, the results of the assessments clearly demonstrate the

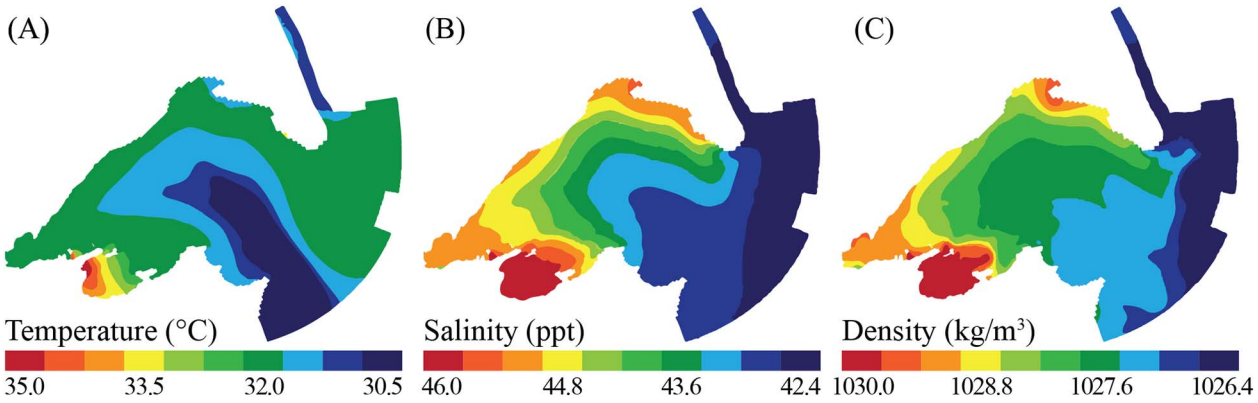

Fig. 13. Mean horizontal distributions of A. temperature, B. salinity, and C. density of the Bay during the summer.

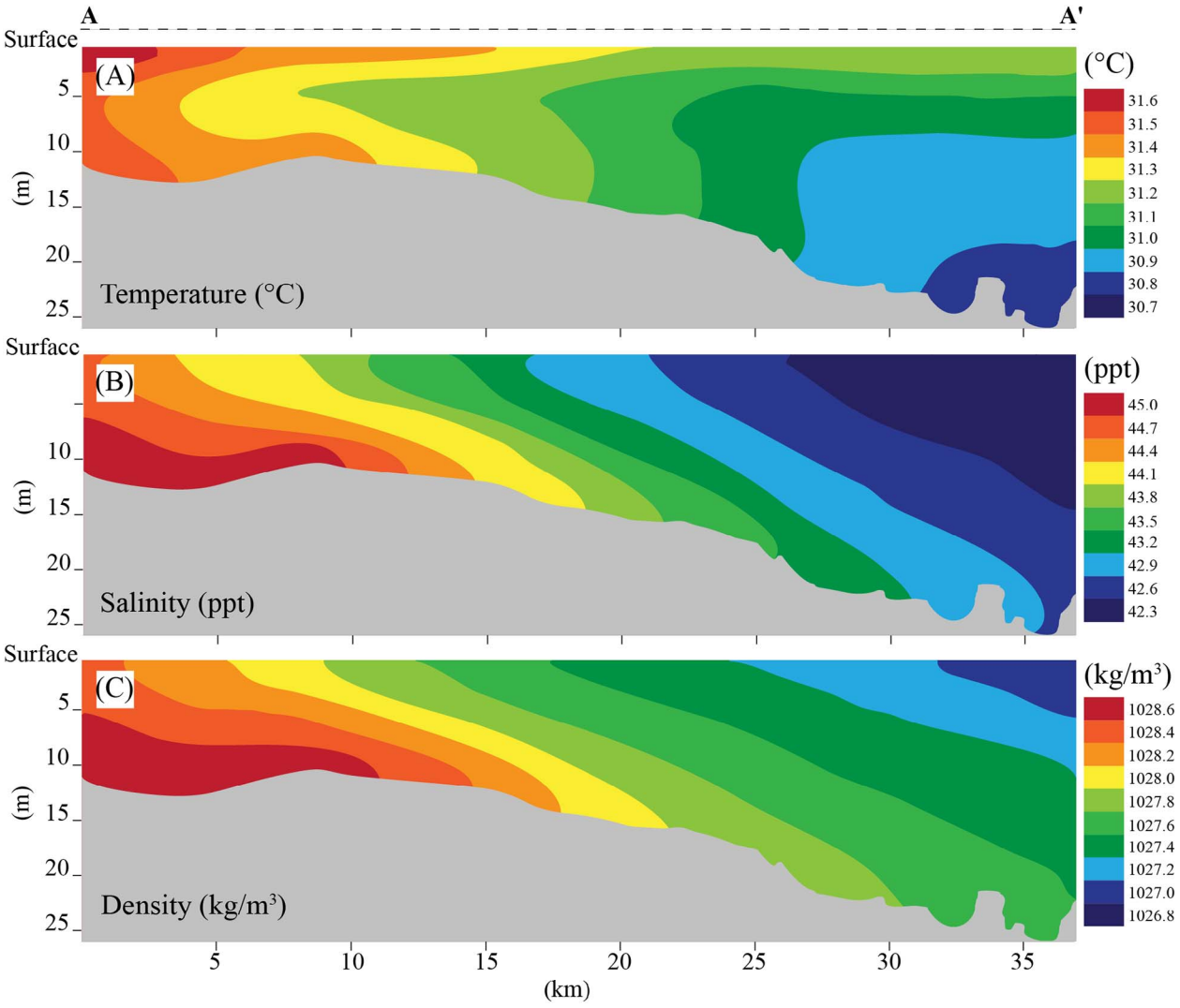

Fig. 14. Mean vertical distributions along the A-A′ section of A. temperature, B. salinity, and C. density of the Bay during the summer.

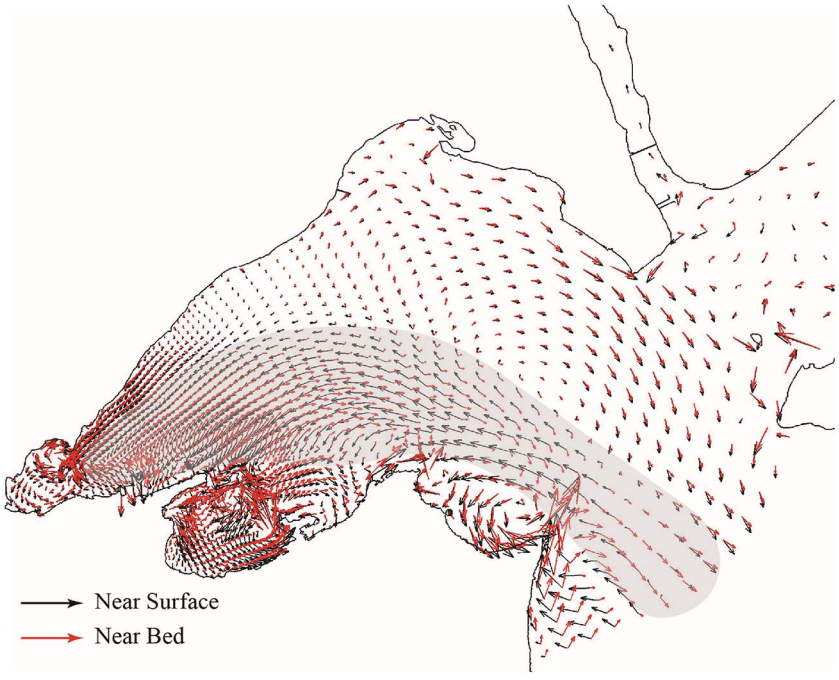

Fig. 15. The residual velocity near the surface and near the bed in the Bay; the shaded area denotes the reverse estuarine circulations, and the scale of the arrow indicates the strength of the currents.

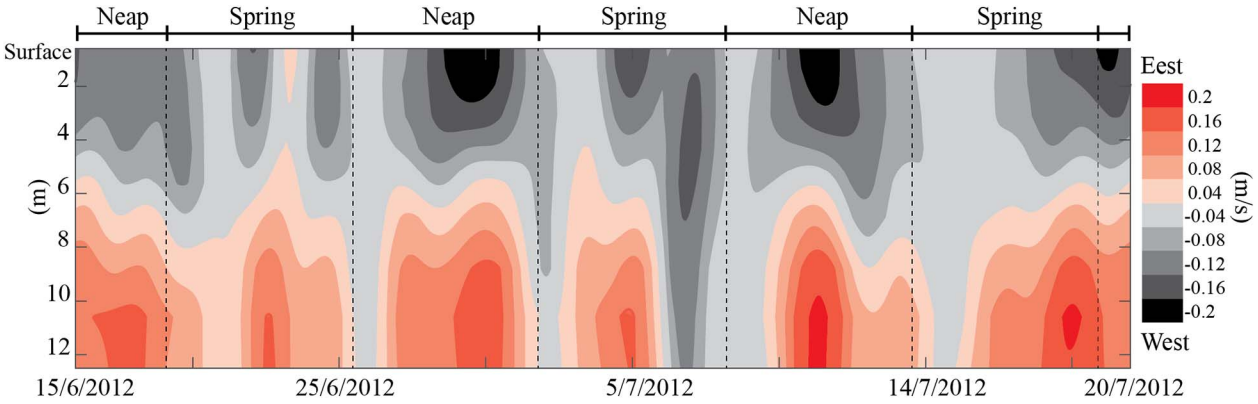

Fig. 16. Residual velocity of the east-west velocity component at station RE.

reverse estuarine conditions at the RE stations (Fig. 16). Almost half of the water column is characterized by landward flow (west of the Bay), while the remaining is in the seaward direction (east of the Bay), which is associated with the differences in the water masses throughout the water column. The results also depict that strong residual flows are created through a series of pulses with variability over the spring-neap cycle (Fig. 16). The formation of those conditions is linked with the interactions of longitudinal shear, partial stratification and mixing during the spring-neap cycle or at shorter time scales. In general, two fundamental mechanisms are responsible for creating the reverse estuarine exchange flows: baroclinic and barotropic flows. The baroclinic flows are driven by the pressure gradients associated with the longitudinal density gradient, as seen previously in Fig. 14C, while the barotropic flows are driven by the tidal pressure gradients but depend on asymmetries in the level of turbulent mixing to produce asymmetric velocity profiles in a typical tidal cycle (Stacey et al., 2001). Having that in mind, the baroclinically driven exchange flows are more pronounced during the neap cycle than the spring cycle when barotropic conditions are more evident at RE station (Fig. 16). Such findings are well aligned with Jay and Smith's (1990) arguments that circulations in the estuary are tied to the spring-neap cycle due to variations in tidal mixing. In the presence of a longitudinal density gradient moving from landward to seaward (Figs. 13 and 14), the tides play a key role in straining the density fields in the opposing direction, particularly during the flood tides. However, with additional straining during spring tides, turbulent fields and the relatively large longitudinal shear forces disturb the isohaline structure and lead to weakening of the reverse circulations. In addition to that, large lateral wind stresses, typically Shamal winds (Fig. 2), enhance mixing and contribute significantly in forming an intermittently well-mixed water column, as seen in Fig. 16.

The case that the inverse residual flows is created through a series of pulses has several implications on the transport of water quality parameters in the Bay and exchange with the Gulf. If a given material in the Bay has time variability in its concentration that is also linked with the spring-neap cycle, then the relative phasing between its concentration and residual-creating flow will be crucial in determining the overall transport. Taking suspended particles as an example, if marked residual flows are only created during neap tides, when suspended particle are also minimal, then the net transport of those particles will be much less than if the residual flow was a constant background circulation. Other flow conditions at the offshore regions also contribute to the exchange regime of the Bay. Peak discharges of Shatt Al Arab play a key role in intensifying the landward currents, as indicated in greyscale in Fig. 16, and consequently have multiple implications to the ecosystem.

The following points summarizes the key works and findings of the current study:

- The hydrodynamic features of the Bay were studied using a numerical model named Delft3D-FLOW and validated with extensive field measurements that cover large areas of the study region during the summer season. The field measurements include profile casting and time series that lasted for more than a typical spring-neap cycle. The main physical parameters considered in the study are water levels, velocity, temperature, salinity and density. The model considers the combined effects of tides, buoyant discharges, and winds to simulate the hydrodynamic processes in a three-dimensional manner. The results show that the model is able to precisely reproduce the barotropic flows and adequately simulate the heat and salt transport.
- The validated model enabled detailed assessment of the temporal and spatial variations of the physical parameters in the Bay in a comprehensive manner using Fourier Analyses.
- Relatively high tidal variations of > 4 m produced a distinctive arrangement of velocity fields in the Bay from near to the shore to the offshore regions. Near the coastline and the headlands of Kuwait City, a clear turbulent regime, associated with eddies, is formed due to the strong interaction of the tidal current. In comparison, a relatively lower dynamic feature dominated the semi-enclosed regions of Sulaibikhat and Jahra Bays.
- At the offshore regions, the strongest uniform currents during the ebb-flood tidal cycle are found at the main axis of the Bay, which reached almost 1 m/s during spring tides. In a similar context, flood tides were found to be relatively stronger then ebb tides.
- The mean variations of the water temperature during summer were found to be highest at Sulaibikhat Bay near the plant discharges. Most distinctive, the mean temperature reached 35 °C in Sulaibikhat Bay, while it was lower by 4 °C at the offshore regions.
- The mean variations of the salinity during summer were found to be highest at the semi-enclosed region, particularly in Sulaibikhat Bay, where it reached 46 ppt; this area is considered the main source of high-salinity fluid for the remaining southern coast of the Bay.
- The variations of the water density followed similar trends as the salinity. The mean density gradually increased from 1026 to 1030 kg/m^3 from the boundary to the inner portions of the Bay, respectively.
- Vertically along the main axis of the Bay, a clear dense front associated with high salinity is formulated near the bed, while lighter waters were present at the surface. For the temperature, cooler waters occupied the deeper portions near the mouth of the Bay and were overlaid with relatively warmer waters; however, the shallow regions were relatively mixed throughout the depth but warmer towards the enclosed areas.
- Residual circulation assessments revealed that the Bay experiences reverse estuarine circulations at the main axis, as illustrated in Fig. 17. Those circulations are mainly associated with two water masses.
- The northern half of the Bay is characterized by clockwise circulations with higher current near the mouth compared to the coastal

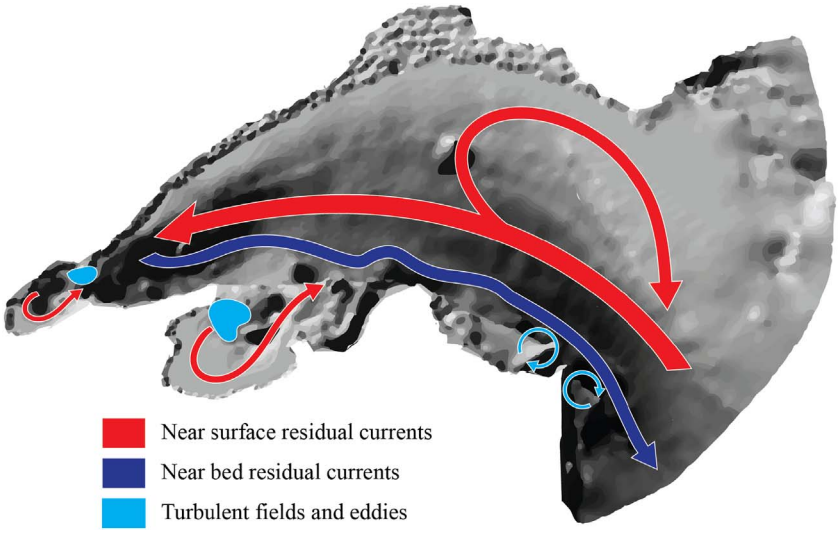

Fig. 17. Overall residual circulations of Kuwait Bay during the summer season; the arrow scale indicates the relative strength of the currents.

areas, while the surface currents are more dynamic than the lower layers (as illustrated in Fig. 17).

- The flows in Sulaibikhat and Jahra Bays are mainly in the counter-clockwise direction, while complex flow fields are existent at the entrance of those embayments due to the interactions of the dense waterfronts with the tidal currents.
- The temporal assessments of the residual currents revealed the variability of the inverse estuarine circulations over the spring-neap cycles in the form of a series of pulses. During the neap cycle, the reverse estuarine circulations are stronger than during the spring cycle due to the mixing and turbulence associated with the tidal currents.
- The spring-neap cycle determined the strength of the baroclinic circulations in the Bay, and they are mainly responsible for the periodic generations of inverse conditions at various strengths. Saline fluids inside the Bay and the relative freshwater outside the Bay formulate density gradients that assist in water exchange with the Gulf waters.
- Shamal winds play a role in creating well-mixed conditions intermittently along the main axis of the Bay.
- Inverse estuarine circulations may not necessarily remain at all times at the main axis of the Bay. Strong seasonal rainfall, reduction of brine waste discharge and other climatic effects may perhaps minimize such conditions.
- Since the main reverse estuarine circulations are concentrated at the southern coast of the Bay where Kuwait City, including economical, commercial and recreational activities, is located, special attention must be given to the surface inflows. The implications of understanding reverse estuarine circulation behaviour are thus broad, ranging from the concerns of dealing with local pollutions to overall management of the ecosystem.

Acknowledgement

This study was mainly supported by the Kuwait Foundation for the Advancement of Sciences (Project No. 2012-1401-01) and Kuwait Institute for Scientific Research (EC060C). Additionally, special thanks are given to the technicians who were heavily involved in the field surveys; their works are greatly appreciated.

References

Al-Banaa, K., Rakha, K., 2009. Seasonal variability of temperature measurements in a shallow bay. J. Coast. Res. 782–786.
Al Senafi, F., Anis, A., 2015. Shamals and climate variability in the Northern Arabian/Persian Gulf from 1973 to 2012. Int. J. Climatol. 35 (15), 4509–4528.
Alosairi, Y., Pokavanich, T., 2017a. Seasonal circulation assessments of the Northern Arabian/Persian Gulf. Mar. Pollut. Bull. 116 (1), 270–290.
Alosairi, Y., Pokavanich, T., 2017b. Residence and transport time scales associated with Shatt Al-Arab discharges under various hydrological conditions estimated using a numerical model. Mar. Pollut. Bull. 118 (1), 85–92.
Alosairi, Y., Imberger, J., Falconer, R.A., 2011. Mixing and flushing in the Persian Gulf (Arabian Gulf). J. Geophys. Res. Oceans 116 (C3).
Alosairi, Y., Pokavanich, T., Al-Salem, K., Taqi, A., Al-Said, T., Al-Hashem, A., Al-Rubaiaan, E., Karam, Q., Al-Yaegoub, A., Al-Dousari, N., Al-Awadhi, S., Al-Houti, D., Shuhaibar, B., 2015. The Optimal and Sustainable Extension of the Emergency Outfalls Along Kuwait Coastline. Kuwait Institute for Scientific Research, pp. 12782 Report No. KISR.
Alosairi, Y., Al-Sulaiman, N., Neelamani, S., Pokavanich, T., Polikarpov, I., Kwarteng, A., Small, S., Al-Handal, A., 2016. Effects of Developments in Mesopotamian Marshland on Boubyan and Warba Islands. Kuwait Institute for Scientific Research, pp. 13610 Report No. KISR.
Al-Rashidi, T.B., Amos, C.L., El-Gamily, H.I., 2007, June. Utilization of remotely sensed data to detect anthropogenic impacts on sea surface temperature of Kuwait Bay, Kuwait. In: OCEANS 2007-Europe. IEEE, pp. 1–5.
Al-Sharhan, A.S., Rizk, Z.A., Nairn, A.E.M., Bakhit, D.W., Alhajari, S. A. (Eds.)., 2001. Hydrogeology of an Arid Region: The Arabian Gulf and Adjoining Areas: The Arabian Gulf and Adjoining Areas. Elsevier.
Boon, J.D., 2006. World Tides User Manual v1.01, USA. (24 pp).
Boon, J.D., 2013. Secrets of the Tide: Tide and Tidal Current Analysis and Predictions, Storm Surges and Sea Level Trends. Elsevier.
Deltares, 2011. Delft3D-FLOW User Manual Simulation of Multi-dimensional Hydrodynamic Flows and Transport Phenomena, Including Sediments, User Manual, Hydro Morphodynamics, Version: 3.15.
Elhakeem, A., Elshorbagy, W., Bleninger, T., 2015. Long-term hydrodynamic modeling of the Arabian Gulf. Mar. Pollut. Bull. 94 (1), 19–36.
Elshorbagy, W., Azam, M.H., Taguchi, K., 2006. Hydrodynamic characterization and modeling of the Arabian Gulf. J. Waterw. Port Coast. Ocean Eng. 132 (1), 47–56.
Glibert, P.M., Landsberg, J.H., Evans, J.J., Al-Sarawi, M.A., Faraj, M., Al-Jarallah, M.A., ... Shoemaker, C., 2002. A fish kill of massive proportion in Kuwait Bay, Arabian Gulf, 2001: the roles of bacterial disease, harmful algae, and eutrophication. Harmful Algae 1 (2), 215–231.
Hamoda, M.F., 2001. Desalination and water resource management in Kuwait. Desalination 138 (1–3), 385–393.
Jay, D.A., Smith, J.D., 1990. Residual circulation in shallow estuaries 2. Weakly stratified and partially mixed estuaries. J. Geophys. Res. 95, 733–738.
Kämpf, J., Ellis, H., 2014. Hydrodynamics and flushing of Coffin Bay, South Australia: a small tidal inverse estuary of interconnected bays. J. Coast. Res. 31 (2), 447–456.
Murakami, M., Oonishi, Y., Kunishi, H., 1985. A numerical simulation of the distribution of water temperature and salinity in the Seto Inland Sea. J. Oceanographical Soc. Jpn. 41 (4), 213–224.
Pokavanich, T., Alosairi, Y., 2014. Summer flushing characteristics of Kuwait Bay. J. Coast. Res. 30 (5), 1066–1073.
Pritchard, D.W., 1967. Observations of circulation in coastal plan estuaries. In: Ward, G., Espey, W. (Eds.), Estuaries. AAAS, Washington, D.C., pp. 37–44.
Rakha, K.A., Al-Banaa, K., Al-Hulail, F., 2010. Flushing characteristics of Kuwait Bay. Kuwait J. Sci. Eng. 37 (1A), 111–125.
Reynolds, R.M., 1993. Physical oceanography of the gulf, Strait of Hormuz, and the Gulf of Oman-results from Mt. Mitchell expedition. Mar. Pollut. Bull. 27, 35–59.
Stacey, M.T., Burau, J.R., Monismith, S.G., 2001. Creation of residual flows in a partially stratified estuary. J. Geophys. Res. Oceans 106 (C8), 17013–17037.
Weisberg, R.H., Zheng, L., 2006. Circulation of Tampa Bay driven by buoyancy, tides, and winds, as simulated using a finite volume coastal ocean model. J. Geophys. Res. Oceans 111 (C1).